Published in final edited form as:
J Comp Neurol. 2008 November 10; 511(2): 271–285. doi:10.1002/cne.21835.

CHANGES IN APICAL DENDRITIC STRUCTURE CORRELATE WITH SUSTAINED ERK1/2 PHOSPHORYLATION IN MEDIAL PREFRONTAL CORTEX OF A RAT MODEL OF DOPAMINE D_1 RECEPTOR AGONIST SENSITIZATION

Sophia T. Papadeas[*,1,2], **Christopher Halloran**[2], **Thomas J. McCown**[2,3,4], **George R. Breese**[1,2,4,5], and **Bonita L. Blake**[2,4,5]

[1]GRADUATE PROGRAM IN NEUROBIOLOGY, SCHOOL OF MEDICINE, UNIVERSITY OF NORTH CAROLINA at CHAPEL HILL, CHAPEL HILL, NC 27599

[2]BOWLES CENTER FOR ALCOHOL STUDIES, SCHOOL OF MEDICINE, UNIVERSITY OF NORTH CAROLINA at CHAPEL HILL, CHAPEL HILL, NC 27599

[3]GENE THERAPY CENTER, SCHOOL OF MEDICINE, UNIVERSITY OF NORTH CAROLINA at CHAPEL HILL, CHAPEL HILL, NC 27599

[4]DEPARTMENT OF PSYCHIATRY, SCHOOL OF MEDICINE, UNIVERSITY OF NORTH CAROLINA at CHAPEL HILL, CHAPEL HILL, NC 27599

[5]DEPARTMENT OF PHARMACOLOGY, SCHOOL OF MEDICINE, UNIVERSITY OF NORTH CAROLINA at CHAPEL HILL, CHAPEL HILL, NC 27599

Abstract

Rats lesioned with 6-hydroxydopamine (6-OHDA) as neonates exhibit behavioral and neurochemical abnormalities in adulthood that mimic Lesch-Nyhan disease, schizophrenia and other developmental disorders of frontostriatal circuit dysfunction. In these animals, a latent sensitivity to D_1 agonists is maximally exposed by repeated administration of dopamine agonists in the post-pubertal period (D_1 priming). In neonate-lesioned, adult rats primed with SKF-38393, we found selective, persistent alterations in the morphology of pyramidal neuron apical dendrites in the prelimbic area of the medial prefrontal cortex (mPFC). In these animals, dendrite bundling patterns and the typically straight trajectories of primary dendritic shafts were disrupted, whereas the diameter of higher-order oblique branches was increased. Although not present in neonate-lesioned rats treated with saline, these morphological changes persisted at least 21 days after repeated dosing with SKF-38393, and were not accompanied by markers of neurodegenerative change. A sustained increase in phospho-ERK immunoreactivity in wavy dendritic shafts over the same period suggested a relationship between prolonged ERK phosphorylation and dendritic remodeling in D_1-primed rats. In support of this hypothesis, pretreatment with the MEK1/2-ERK1/2 pathway inhibitors PD98059 or SL327, prior to each priming dose of SKF-38393, prevented the morphological changes associated with D_1 priming. Together, these findings demonstrate that repeated stimulation of D_1 receptors in adulthood interacts with the developmental loss of dopamine to profoundly and persistently modify neuronal signaling and dendrite morphology in the mature prefrontal cortex. Furthermore, sustained elevation of ERK

Correspondence: Bonita L. Blake, D.V.M., Ph.D., 3010 Thurston-Bowles Bldg., CB# 7178, Bowles Center for Alcohol Studies, Chapel Hill, NC 27599-7178, Phone 919-966-0505, Fax: 919-966-5679, email: bonita_blake@med.unc.edu.
[*]**Current address for Dr. Papadeas:** Sophia Papadeas, Ph.D., The Johns Hopkins University, Department of Neurology, 600 North Wolfe Street, Meyer 6-144, Baltimore, MD 21287-0005

activity in mPFC pyramidal neurons may play a role in guiding these morphological changes *in vivo*.

Keywords

Prefrontal cortex; dendrites; neonatal 6-hydroxydopamine; sensitization; ERK

INTRODUCTION

Dendrites receive multiple and diverse synaptic inputs, processing and integrating them into signals that convey information to the soma and axon. Neuronal identity largely dictates basic dendrite structure, but environmental signals further shape dendrites during development and in adulthood (Miller and Kaplan, 2003). In a reciprocal manner, dendritic morphology impacts spatial and temporal neurotransmission by affecting the propagation and patterning of action potentials (Mainen and Sejnowski, 1996; Vetter et al., 2001). Accordingly, the structural remodeling of dendrites and their spines is thought to coordinate with physiological processes associated with neuroadaptation, such as learning and memory (Lamprecht and LeDoux, 2004) and behavioral sensitization to psychostimulants (Robinson and Kolb, 2004).

The neonatal administration of 6-OHDA to rats results in behavioral, functional and neurochemical effects that are different from those of rats lesioned with 6-OHDA in adulthood (Breese et al., 2005). One consequence of neonatal lesioning is a latent behavioral sensitivity to D_1 dopamine receptor agonists that is only maximally expressed following repeated, post-pubertal dopamine agonist administration (Criswell, 1989). This phenomenon, known as "D_1-priming", results in a profound activation of locomotor and stereotypical behaviors in response to doses of the D_1 agonist SKF-38393 that are behaviorally ineffective in control rats. While these agonist-induced hyperactive behaviors abate within a few hours of dosing, the increased sensitivity to a subsequent agonist challenge lasts for at least 6 months (Breese et al., 1984; Criswell et al., 1989). Importantly, neonate-lesioned rats dosed repeatedly with saline in early adulthood exhibit normal baseline activity and low to moderate behavioral sensitivity to a single challenge with SKF-38393. These findings suggest that, when superimposed upon the developmental effects of reduced dopamine, repeated D_1 agonist exposure in neonate-lesioned rats stimulates long-lasting neuroadaptive changes that mediate the profound behavioral sensitivity of these animals.

Recently, we demonstrated the remarkably persistent phosphorylation of ERK1/2 and CREB in medial prefrontal cortex (mPFC) neurons of D_1-primed rats (Papadeas et al., 2004), and proposed that such sustained activation of neuronal signaling may promote enduring neuroplastic changes in this region. In the current report, we describe modifications in the morphology of pyramidal neuron apical dendrites that accompany prolonged ERK phosphorylation in the mPFC of these animals. Furthermore, by blocking these morphological changes with MEK1/2 inhibitors administered *in vivo*, evidence is provided to suggest these structural adaptations are supported by activity of the ERK1/2 signaling pathway.

MATERIALS AND METHODS

Drugs

6-hydroxydopamine hydrobromide (6-OHDA; ICN, Irvine, CA) was dissolved in saline containing 0.5% ascorbic acid. Desipramine HCl (Sigma-Aldrich, St. Louis, MO) and

SKF-38393 (2,3,4,5-tetrahydro-7,8-dihydroxy-1-phenyl-1H-3-benazepine HCl; Sigma-Aldrich), were dissolved in saline. SL327 (α-[amino[(4-aminophenyl)thio]methylene]-2-(trifluoromethyl) benzeneacetonitrile; a gift from Bristol-Myers-Squibb Company, Princeton, NJ) and PD98059 (2′-amino-3′-methoxyflavone; Calbiochem, La Jolla, CA) were dissolved in dimethylsulfoxide (DMSO) and further diluted in sterile saline (pH 7.3) to a concentration of 1% DMSO immediately prior to intracerebroventricular (icv) infusion (Gu et al., 2001). For intraperitoneal (ip) administration, SL327 was dissolved in DMSO at 2 mg/ml as described by Atkins et al. (1998). Kainic acid (Sigma-Aldrich, St. Louis, MO) was dissolved in saline at 1 mg/ml. Drug dosages are provided below.

Experimental Design

All animals were treated and used in accordance with the *NIH Guide for the Care and Use of Laboratory Animals* with approval from the Institutional Animal Care and Use Committee at UNC-Chapel Hill. Sprague-Dawley rats were bred in-house from stock obtained from Charles River Labs, Raleigh, NC. To lesion dopaminergic neurons, rats were injected intracisternally with 6-OHDA (neonate-lesioned) on postnatal day (PND) 4 as previously described (Papadeas et al., 2004). Sham-lesioned rats were injected with saline. In both groups, noradrenergic neurons were protected by administering a single dose of desmethylimipramine (20 mg/kg ip) 1 hour prior to lesioning. Both sexes were used for the present study, balanced with the same number of controls of each sex. There were no gender differences in locomotor behavior or morphological findings (data not shown).

A timeline of experimental procedures is provided in Fig. 1. Beginning on PND 42, rats were administered four ip injections of the selective, partial D_1 agonist SKF-38393 (3 mg/kg) or saline vehicle at weekly intervals (Fig. 1A, *Basic Protocol*). The use of SKF-38393 for this study is based on a significant body of data from our laboratory relating to the behavioral effects of this agonist in the neonate lesioned rat (for example, see Breese et al., 1985;Criswell et al., 1989;Criswell et al., 1990;Moy et al., 1994;Papadeas et al., 2004), including a previous study demonstrating higher efficacy of SKF-38393 in producing locomotor activation and lower potency to produce self-injurious behavior compared to a selective, full D_1 agonist (Johnson et al., 1992). In addition, this dose of SKF-38393 does not stimulate locomotor activity or induce behavioral sensitization in sham-lesioned rats (Criswell et al., 1989;Moy et al., 1994;Papadeas et al., 2004, and see below). As described previously (Papadeas et al., 2004), behavioral sensitivity to SKF-38393 administration (D_1 priming) was monitored following each dose, and neonate-lesioned rats exhibited a progressive increase in agonist-mediated locomotor activity culminating in ≥80,000 total horizontal counts/180 min following the final SKF-38393 treatment. Activity counts of neonate-lesioned rats treated with saline and sham-lesioned rats treated with either saline or SKF-38393 typically ranged from 1500 to 3000 total counts/180 min. It is important to note that the spontaneous locomotor activity of D_1-primed rats is similar to that of the controls. In other words, neonate-lesioned adults that have already received repeated doses of SKF-38393 are behaviorally supersensitive to the locomotor activating effects of a subsequent injection of the D_1 agonist, but they do not exhibit locomotor hyperactivity when injected with saline (1500 to 3000 activity counts/180 min), nor in the absence of manipulation in the home cage (data not shown). Relative to saline-treated rats, the weekly episodes of drug-induced hyperactive behavior did not affect the physical appearance, body weight, or weight gained per week of lesioned, SKF-38393-treated rats (data not shown).

Some rats were surgically implanted with icv cannulae before agonist dosing in preparation for administering inhibitors of MEK1/2 (Fig. 1B, *MEK inhibitor preinfusions*). At PND 35, drug-naïve neonate-lesioned and sham-lesioned rats were anesthetized with sodium pentobarbital (50 mg/kg, ip) and sterotaxically implanted with a 26-gauge stainless steel cannula into the right lateral ventricle (from bregma; anteroposterior, -0.8 mm; mediolateral,

-1.5 mm; dorsoventral, -2 mm; according to Paxinos and Watson (1998). The cannula was fixed in place with dental cement and the animals were allowed to recover for 7 days before initiating the D_1 agonist treatment. Beginning on PND 42, animals received icv infusions of PD98059 (0.38 nmol/μl), SL327 (1 nmol/μl) or vehicle (1% DMSO in sterile saline), prior to each weekly systemic dose of SKF-38393. A 32-gauge stainless steel microinjector needle and variable-rate syringe pump were used to inject a volume of 2 μl over 5 min intraventricularly. The needle was allowed to remain in place for 1 min to reduce backflow of the solution along the injection track. After 30 min, D_1 agonist injections were followed by behavioral testing as described above.

In a third experiment (Fig. 1C, *AAV-GFP transduction*), prelimbic neurons of some animals were transduced *in vivo* with green fluorescent protein (GFP) prior to initiating the priming regimen with SKF-38393. This allowed us to directly visualize the changes in dendritic structure caused by D_1-priming when brain sections were later examined microscopically. Preparation and infusion of the adeno-associated virus (AAV) vector construct, with expression of GFP driven by a hybrid chicken beta-actin promoter (AAV-GFP), has been described (McCown et al., 2006). Briefly, drug-naive neonate-lesioned and sham-lesioned rats were anesthetized on PND 30 with sodium pentobarbital as described above and placed in a Kopf stereotaxic apparatus. A 33-gauge injector was lowered into the prelimbic area (from bregma; anteroposterior, 3.2 mm; mediolateral, -0.6 mm; dorsoventral, -2.0 mm; according to Paxinos and Watson, 1998). Using a Sage syringe pump (Thermo Electron Corporation, Beverly, MA), 2.0 μl of recombinant vector (titer, 1×10^{13} viral particles/ml) was microinfused over a 20 min period into the mPFC. The injector was left in place for 3 min post-infusion to allow diffusion from the site and to prevent backflow of solution. The incision was closed and animals were allowed 12 days to recover from the infusions before the D_1 agonist dosing was initiated. AAV-GFP-transduced cells continue to express GFP for several months *in vivo* (Klein et al., 2002). In the present study, vivid GFP expression was evident at day 7 after the final weekly treatment with SKF-38393 (approximately 40 days after viral-mediated transfer).

In the fourth experiment, rats that had been transduced with AAV-GFP at 30 days of age received systemic injections of SL327 (100 mg/kg, ip) prior to each dose of D_1 agonist (Fig. 1D, *AAV-GFP + systemic MEK inhibitor*). Systemic administration of this blood-brain barrier-permeable MEK inhibitor substantiated the results we obtained with icv infusion of SL327 and furthermore, obviated the need for dual surgeries for cannula implantation and intracortical viral injections. SL327 was administered 30 min prior to the weekly SKF-38393 injections and behavioral testing was performed as described above for four weeks.

In all studies, rats were euthanized on PND 70 (7 days after the final priming treatment) by transcardial perfusion with 4% paraformaldehyde as previously described (Papadeas et al., 2004) or by decapitation. One exception was a subset of animals in the Basic Protocol (3-4 per group), perfused on day 84 (21 days after the final agonist dose) to assess the persistence of the morphological effects.

Antibody characterization

Affinity-purified, polyclonal anti-tyrosine hydroxylase (TH) antibody (#657012, Calbiochem, San Diego, CA) was raised in rabbits against purified, SDS-denatured rat pheochromocytoma TH enzyme. This antibody recognizes a single band of approximately 60 kDa on Western blots of rat striatum or PC-12 cell extracts (Haycock, 1989). Specificity for tyrosine hydroxylase by immunohistochemistry is demonstrated by the loss of immunoreactivity in rat striatum after lesioning of dopaminergic afferents with 6-OHDA (Papadeas et al., 2004).

Anti-phospho-p44/42 MAP kinase (Thr202/Tyr204) (#9106, Cell Signaling Technology, Beverly, MA) is a mouse monoclonal antibody raised to a synthetic keyhole limpet hemocyanin (KLH)-conjugated phosphopeptide corresponding to amino acid residues 198-208 of human p44 MAP kinase (ERK1), containing the Thr202/Tyr204 phosphorylation sites (Thr-Gly-Phe-Leu-pThr-Glu-pTyr-Val-Ala-Thr-Arg-Trp-Tyr-Arg-Cys). According to Cell Signaling Technology, the antibody reacts specifically with as little as 50 pg of phosphorylated ERK and does not cross-react with up to 4 μg of nonphosphorylated ERK by Western blotting. It selectively recognizes two distinct bands at approximately 44 kDa and 42 kDa corresponding to ERK1 and ERK2, respectively (per the manufacturer and our previous data, not shown). As immuohistochemical controls in the present study, a 10-fold (w/w) excess of phosphorylated or non-phosphorylated immunizing peptide (#ab5255, Abcam, Cambridge MA) was preadsorbed with the antibody overnight (with gentle shaking at 4°C) prior to labeling tissue sections by the standard immunohistochemical and antigen retrieval protocols described below. No signal was detected when the antibodies were preadsorbed with phosphorylated peptide prior to staining sections by the standard protocol (not shown) or by antigen retrieval (Fig. 5C, *Phosphopeptide*). On the other hand, the non-phosphorylated peptide failed to block immunohistochemical labeling with the antibody, either on sections stained by the standard method (not shown), or using antigen retrieval (Fig. 5C', *Non-phosphopeptide*). Thus the antibody recognizes the phosphorylated, but not the non-phosphorylated, form of ERK1/2. Further controls were run by staining sections in the absence of primary antibody under standard and antigen retrieval conditions; phospho-ERK staining was not observed and the results appeared similar to that seen in Fig. 5C, *Phosphopeptide*. It should be noted that Cell Signaling Technology no longer recommends product #9106 for immunohistochemistry, advising that newer products may be more suitable for this procedure.

The mouse monoclonal anti-MAP2 antibody (clone AP20; #MAB3418, Chemicon, Temecula, CA) was raised to purified MAP2 from bovine brain. On Western blots this antibody recognizes two closely associated bands of approximately 300 kDa, corresponding to the high molecular weight (HMW) forms of MAP2 (MAP2a and MAP2b). It does not react with the low molecular weight (LMW) form known as MAP2c, or with MAP1 (Binder et al., 1986; Kalcheva et al., 1994; Blanchart et al., 2006; this study). The AP20 clone has been used extensively to detect MAP2 in rat brain sections and specifically labels neuronal dendrites and somata (see for example, Minger et al., 1998; Bury and Jones, 2002). Immunohistochemical controls for the present study consisted of rat brain coronal sections stained in the absence of primary antibody; no tissue labeling was apparent with the use of either biotinylated or fluorescence-conjugated secondary antibody (see below; data not shown).

A mouse monoclonal antibody to αII-spectrin (α-fodrin, clone AA6; #mab1622, Chemicon) was generated to the purified membranes of lysed, enucleated chicken red blood cells. According to the manufacturer, it is specific for the 240 kDa full-length α-spectrin protein found in all mammalian nonerythroid cells, and recognizes α-spectrin breakdown products (SBDPs) generated through cleavage by caspase (150 kDa, 120 kDa) and calpain (150 kDa). Several studies have utilized this product to characterize caspase and calpain activation in rat cortex (Rau et al., 2003; Carloni et al., 2004; Calon et al., 2005) and other tissues.

The mouse monoclonal anti-β-actin antibody (clone AC-15; #A5441, Sigma-Aldrich) was generated to a slightly modified synthetic peptide corresponding to the N-terminus of cytoplasmic β-actin (Acetyl-Asp-Asp-Asp-Ile-Ala-Ala-Leu-Val-Ile-Asp-Asn-Gly-Ser-Gly-Lys), coupled to KLH. It recognizes a single band at 42-45 kDa in a variety of tissues (per the manufacturer). Its use as a reagent to normalize protein loading in Western blotting has been characterized (Liao et al., 2000).

Immunohistochemistry (IHC) and Western blotting (WB)

Immunohistochemical staining methods were performed as previously described (Papadeas et al., 2004) on 40 μm free-floating coronal vibratome sections. In some cases, adjacent sections were mounted and stained with 0.1% cresyl violet to study the cytoarchitecture. Tyrosine hydroxylase immunoreactivity (1:4000 for IHC) was determined to establish the extent of 6-OHDA lesioning (not shown). Anti-phospho-p44/42 MAP kinase (1:500) was used to detect phospho-ERK. For qualitative evaluation of phospho-ERK staining in dendrites, antigen retrieval was performed to enhance phospho-ERK1/2 staining in the mPFC. The free-floating tissue sections were incubated at 70°C in 10 mM sodium citrate buffer, pH 8.5 for 30 minutes, then washed once in 0.1M phosphate buffered saline, pH 7.4 (PBS) prior to immunostaining. Other sections were processed for phospho-ERK (1:500) without antigen retrieval for quantitative evaluation by cell counting. All TH- and phospho-ERK-stained sections were processed using Vectastain Elite ABC kits (rabbit IgG, #PK-6101; mouse IgG, #PK-6102; Vector Laboratories, Burlingame, CA) per the manufacturer's instructions with immunochemical detection using nickel-cobalt intensification of the 3,3′-diaminobenzidine (DAB) reaction product. MAP2A and B were detected using the monoclonal anti-MAP2 antibody (1:500) by DAB IHC (performed with the Vectastain Elite kit as described above) and by immunofluorescence. For fluorescence IHC, free-floating tissue sections were incubated overnight at 4°C with anti-MAP2, followed by incubation in Molecular Probes AlexaFluor 594-conjugated goat anti-mouse secondary antibody (1:500; #A-11032, Invitrogen, Carlsbad, CA) for 45 min at 4°C with agitation.

For Western blotting, brains were rapidly removed immediately following decapitation, and the mPFC was dissected on ice, quickly frozen, and stored at -80°C until use. Tissues were homogenized by sonification in solubilization buffer (10 mM Tris-HCl, 50 mM NaCl, 1% Triton X-100, 30 mM sodium pyrophosphate, 50 mM NaF, 5 nM $ZnCl_2$, 100 μM Na_3VO_4, 1 mM DTT, 5 nM okadaic acid, 2.5 ng/ml aprotinin, 2.5 ng/ml pepstatin, and 2.5 ng/ml leupeptin). Insoluble material was removed by centrifugation (13,000 rpm for 20 min at 4°C), and protein concentration determined using a BCA protein assay kit (Pierce, Rockford, IL). Samples were mixed with Novex Tris-glycine SDS sample buffer (San Diego, CA) containing 5% 2-mercaptoethanol and heated to 90°C for 3 min. Aliquots of 20 μg of protein/lane were separated on Novex 8-16% gradient Tris-glycine gels under reducing conditions. Loading concentrations were based on pilot immunoblots (not shown) to determine densitometric linearity under the detection conditions described below. Proteins were transferred to polyvinylidene difluoride membranes (Immobilon-P, Millipore, Bedford, MA), rinsed 3 times in PBS for 5 min, and incubated in Odyssey Blocking Buffer (LI-COR Biosciences, Lincoln, NE) for 1 hour. Proteins were detected using one of the following: anti-MAP2 antibody (1:500), anti-α-spectrin antibody (1:1000), or anti-β-actin antibody (1:5000), diluted in 50% Odyssey Blocking Buffer in PBS containing 0.1% Tween-20. Binding of the primary antibodies to their respective proteins was detected using Odyssey IRDye 800CW-conjugated goat anti-mouse IgG (1:15,000; #926-32210, LI-COR) or Odyssey IRDye 680-conjugated donkey anti-mouse IgG (1:15,000: #926-32222, LI-COR). Fluorescent signals were detected using the Odyssey Infrared Imaging System (LI-COR Biosciences). Average integrated signal intensity measurements were calculated using Odyssey image analysis software after normalizing to β-actin.

Image acquisition and analysis

Immunohistochemical sections were analyzed by light microscopy using an Olympus BX50 microscope outfitted with a Sony DCX-390 video camera. Light levels were normalized to preset values to ensure fidelity of the data acquisition. Cell counts were collected directly while viewing in a single optical plane with a 20X objective as described previously

(Papadeas et al., 2004) for phospho-ERK immunoreactivity and cresyl violet-stained sections. In the latter, neurons were identified by their larger size and the presence of prominent cresyl violet-stained cytoplasm and euchromatin in the nucleus. Although these criteria may exclude some small neurons, most non-neuronal cells are eliminated from counting. Cortical thickness and laminar measurements were taken from grayscale images of cresyl violet-stained sections at a magnification of 8X, using the straight-line measure function in ImageJ v1.37. Cortical laminae were estimated on the basis of characteristic cytoarchitectonic landmarks as described by Van Eden and Uylings (1985), and Zilles and Wree (1995). Measurements of layers I - VI were summed to obtain an estimate of total cortical thickness. For MAP2 analyses, 8-bit grayscale images spaced approximately 250 μm apart were collected in layers II/III and V of mPFC. Six samples were obtained from each of four different sections per animal. The area fraction of MAP2 immunostained components was estimated using ImageJ software v1.34s. A grayscale morphology plugin (available at http://rsb.info.nih.gov/ij/plugins/gray-morphology.html) was used to apply a closing operator with an arbitrary radius of 6 pixels to each of the digitized images. This enabled us to focus on larger MAP2-positive linear elements (primarily first order dendritic processes) while omitting MAP2-stained somata and other features. The images were held to a consistent threshold such that MAP2-stained dendrites were black and the background was white. Threshold levels were individually set to ensure all MAP2-stained dendrites were identified and image analysis was performed using the 'Analyze Particles' function in Image J. Values were averaged for each animal, and means determined across all animals within a treatment group. Statistical comparisons between groups were carried out with ANOVA. Where appropriate, post-hoc comparisons between groups were performed using a Fisher's PLSD test. Representative light microscopic images for publication were adjusted for color, brightness and contrast in Adobe Photoshop v5.0 and assembled in Adobe Illustrator v9.0.

Confocal imaging was performed at the Michael Hooker Microscopy Center at UNC-Chapel Hill using a Zeiss Axiovert LSM510 laser confocal microscope equipped with argon (488 nm) and HeNe (543) lasers. Images were processed using Zeiss LSM Image Browser and Adobe Photoshop software. MAP2 immunofluorescence and dual-label MAP2 and GFP fluorescence images for qualitative assessment were reconstructed from a minimum of three consecutive steps in a *Z*-series taken at 1 μm intervals through the section of interest using a 40x objective. Images were centered on layer II/III of the prelimbic cortex and included portions of layers I and V (see Fig. 2I). To measure parameters of GFP-positive dendrites, projected stacks of ten such images were analyzed using ImageJ v1.37c. There were no differences in the total number of visible primary shafts or dendrite branches between the groups. Dendrite lengths were traced with a mouse-driven cursor on the computer screen along their visible distance until they bifurcated or left the visible field. In order to control for slight differences in the positioning of photomicrographs, segments with end-to-end lengths shorter than 50 μm and longer than 300 μm were excluded. Curvilinear lengths were measured using the freehand utility, and end-to-end lengths were measured with the straight-line function in ImageJ. The linearity index (LI) was calculated as the ratio of curvilinear length to the distance between ends as described by Demyanenko et al. (1999). Dendrite diameters, measured using the ImageJ straight-line function, represented an average of two to three measurements spaced evenly along each visible segment. Most of the oblique dendrites that were visible in this layer appeared to be secondary or tertiary branches of pyramidal neurons, although some of these processes might have arisen from the few non-primary neurons that expressed GFP. Length and diameter measurements are expressed in micrometers as the mean ± S.E.M. of 3 to 6 rats per group. Total number of length measurements: primary shafts, 20-114 dendrites per rat yielding a total of 192 -213 dendrites per treatment group; layer I branches, 13-68 per rat, 126-204 per group; layer II/III oblique branches, 10-29 per rat, 57 to 65 per group; layer V oblique branches, 10-18 per rat, 40-41 per group. Total diameter measurements: primary shafts, 20-87 per rat, 155-219 per group;

layer I branches, 84-137 per rat, 366-421 per group; layers II/III and V oblique branches, 30-78 per rat, 115-209 per treatment group. Statistical comparisons between treatment groups were carried out with ANOVA with Fisher's PLSD. Representative confocal microscopic images for publication were adjusted for color, brightness and contrast in Zeis LSM Image Browser v3.2.0.115 and assembled in Adobe Illustrator v9.0.

RESULTS

D_1-sensitized rats exhibit altered MAP2 immunostaining in medial prefrontal cortex

In adult rats that have been lesioned with 6-OHDA as neonates, repeated weekly administration of SKF-38393 (3 mg/kg ip) results in behavioral sensitization to the locomotor activating effects of selective D_1 agonists. In these "D_1-primed" animals, a challenge dose of SKF-38393 elicits enhanced ambulatory and stereotypical behaviors, even when administered months later (Criswell et al., 1989; Criswell et al., 1990). This behavioral activation by SKF-38393 is transient (lasting approximately 3 hours post-injection), and in the absence of drug administration, spontaneous locomotor activity in adults is similar to that of sham-lesioned rats. Sham-lesioned rats do not exhibit locomotor activation following acute SKF-38393 injections at this dose, nor do they become behaviorally sensitized or primed to the agonist with repeated systemic administration (Criswell et al., 1989). Not surprisingly then, when MAP2A/B immunohistochemistry was performed on day 7 after the basic treatment protocol, dendritic MAP2 staining profiles were similar in all sham-lesioned rats whether they were treated with SKF-38393 (Sham-SKF) or with saline (Sham-Sal). In mPFC of these animals, MAP2 antibodies stained apical dendrites of layers II/III and V pyramidal neurons intensely (Fig. 2A & B). First-order dendritic shafts were long and straight, and traversed from deeper layers of the cortex to the pial surface in well-delineated bundles, in agreement with descriptions by Gabbot and Bacon (1996). Likewise, day 7 tissue sections from neonate-lesioned rats injected repeatedly with saline in adulthood (Les-Sal) demonstrated classic mPFC MAP2 profiles that were indistinguishable from those of sham-lesioned animals (Fig. 2C). On the other hand, D_1 priming of neonate-lesioned rats by repeatedly injecting SKF-38393 during adulthood (Les-SKF) resulted in MAP2-stained apical dendritic processes that were shorter and bent, and bundling was far less prominent (Fig. 2D). In Les-SKF animals, immunostaining in the neuropil throughout mPFC cortical layers II through VI was attenuated relative to sham-lesioned rats, and layer I was frequently stained more intensely than deeper layers. Although it is difficult to discern in Fig. 2D, the border lying between layers I and II/III was more jagged in Les-SKF rats than the typically straight, even margin of the sham-lesioned groups. At higher magnification in layer II/III (Fig. 2E), Les-SKF dendritic bundles containing at most 2 to 3 visible shafts were observed, and apical dendrites appeared truncated or discontinuous with obvious deviations from the normal straight path. Sections from lesioned rats sacrificed 21 days after the final SKF-38393 treatment (Fig. 2F) were virtually indistinguishable from day 7 sections, with dendritic profiles that continued to course non-uniformly toward cortical layer I.

Immunofluorescence staining revealed several additional aspects of anti-MAP2 labeling that had been less apparent with the DAB staining method. Using confocal microscopy to examine the neuropil, small punctuate structures and fine processes consistent with oblique dendrites were observed in layer II/III of Sham-Sal, Sham-SKF and Les-Sal rat mPFC (Sham-SKF, Fig. 2G; Sham-Sal and Les-Sal are not shown). Compared with the fine fibrous arrangement of neuropil in these control groups, the layer II/III neuropil of Les-SKF rats appeared more coarsely textured, with larger punctae and thicker oblique branches (Fig. 2H). At the interface of cortical layers I and II/III, second and third order dendritic branches of pyramidal neurons diverged from the primary shafts and could be followed for some distance into the neuropil of mPFC layer I in Sham-Sal, Sham-SKF and Les-Sal rats. In the

mPFC of Les-SKF rats however, MAP2 immunostained branches appeared thickened and truncated as they diverged and penetrated layer I (Fig. 2H, arrowheads).

The pattern of straight, roughly equidistant parallel bundles of first order apical dendrites is distinctive of pyramidal neurons in the cortex. To determine if the disruption of MAP2 immunostaining by D_1 priming was representative of a widespread effect, cortical regions throughout the brain were examined. With the exception of the anterior cingulate area that caudally adjoins the prelimbic mPFC (not shown), cortical pyramidal neuron dendritic profiles appeared normal throughout as exemplified by MAP2 staining in the visual cortex (Fig. 2J). Likewise, inspection of hippocampal subregions revealed no changes in MAP2 dendritic profiles with D_1 priming (not shown).

Neural insults, such as traumatic brain injury, oxygen-glucose deprivation, and NMDA-dependent excitotoxicity, are frequently accompanied by calcium-dependent proteolysis of MAP2 and other cytoskeletal proteins (Czogalla and Sikorski, 2005). Loss of MAP2 protein by proteolysis might thus explain the diminished DAB immunohistochemical staining in the neuropil of the D_1-supersensitive mPFC, as well as the fragmented appearance of stained apical dendritic processes. In order to quantitatively assess MAP2 protein levels, the same antibodies that were used to label MAP2A/B immunohistochemically were applied to Western blots of microdissected mPFC. The results revealed a characteristic broad band or closely associated doublet of approximately 300kD consistent with MAP2A/B (Fig. 3A). Fainter bands of increased electrophoretic mobility presumably represented MAP2 proteolytic degradation products (Quinlan and Halpain, 1996a). After normalization to β-actin, average integrated signal intensity measurements for 300kD MAP2 were found to be similar across all four treatment groups ($F_{(3,14)} = 0.726$, $p = 0.55$). Likewise, actin-normalized measures of the total remaining lower molecular weight bands in each lane were not different ($F_{(3,14)} = 0.263$, $p = 0.85$). Thus while MAP2 immunoreactivity in histological sections appeared reduced, no loss of total levels of MAP2 protein was detected on Western blots, and there was no evidence of enhanced MAP2 proteolysis. To substantiate the latter findings, we immunoblotted Sham-Sal and Les-SKF mPFC lysates for αII-spectrin (α-fodrin). Accumulated spectrin breakdown products (SBDPs) of 145-150 and 120 kDa are a reliable indicator of recent activation of calpain and caspase-3 proteases, respectively, in damaged neurons (reviewed by Wang, 2000). As shown in Fig. 3B, levels of all SBDPs found in the Les-SKF mPFC were similar to control (SBDPs normalized to full-length spectrin in Les-SKF *vs*. Sham-Sal, $F_{(1,14)} = 0.614$, $p = 0.44$ for 145-150 kDa SBDPs, $F_{(1,14)} = 0.374$, $p = 0.55$ for 120 kDa SBDP). Finally, we examined the cytoarchitecture of cresyl violet-stained coronal sections of the mPFC in each of the four treatment groups at 21 days after the final dose of SKF-38393. There were no significant differences in total cell counts across all layers of the cortex (main effect, $F_{(3,12)} = 0.971$, $p = 0.4385$), nor in the relative distribution of cells in the superficial *vs*. deep layers (Fig. 3C). Likewise, total cortical thickness was not altered (main effect, $F(3,12) = 1.206$, $p = 0.3494$), although the thickness of layers II/III and V was slightly redistributed in 6-OHDA-lesioned animals compared to their sham-lesioned counterparts (Fig. 3D). In these layers, the effects of lesioning (layer II/III, $F_{(1,12)} = 4.099$, $p = 0.658$; layer V, $F_{(1,12)} = 0.499$, $p = 0.4933$) and drug treatment (layer II/III, $F_{(1,12)} = 0.063$, $p = 0.8056$; layer V, $F_{(1,12)} = 0.155$, $p = 0.7004$) did not reach significance, nor was there a significant interaction of lesion condition and drug treatment (layer II/II, $F(1,12) = 0.0002$, $p = 0.9876$).

Taken together, the results described above demonstrate that D_1 priming is associated with long-lasting changes in the dendritic appearance of MAP2 immunohistochemical staining in the mPFC, but not with quantitative changes in MAP2 expression. The disruption of MAP2-positive immunohistochemical profiles is often cited as an indicator of compromised dendritic structural integrity. However, the absence of changes in immunoblotted MAP2

profiles, markers of calcium-dependent proteolysis, total cell counts or laminar thickness collectively suggest that widespread cellular damage or dendrite destruction do not account for the altered appearance of MAP2 in fixed tissue sections. We therefore focused our efforts on determining whether a qualitative change in dendrite morphology might explain these results.

Morphological abnormalities of apical dendrites in mPFC of D_1-sensitized rats

To visualize neurons and their processes directly, a recombinant AAV vector with GFP as the transgene (McCown et al., 2006) was microinjected bilaterally into the mPFC of neonate- and sham-lesioned rats 12 days prior to initiating treatment with SKF-38393. Using low-power fluorescence microscopy, clusters of GFP-positive cell bodies enabled verification that the majority of placements were made in layer V, although a few layer II/III cells could be identified. Most of the GFP-expressing cells were consistent morphologically with pyramidal neurons. Conspicuous apical dendrites could be visualized extending from deeper layers well into layer I (Fig. 4A), however basal dendrites were more difficult to distinguish due to the close arrangement of fluorescent somata and fainter intensity of GFP expression in basal areas. Somal size, although not measured, did not appear to be affected by treatment. Compared to mPFC neurons of Sham-SKF rats, apical shafts of Les-SKF cells originating in layers II/III and V appeared to be wavier and somewhat disorganized. Dendritic spines were sometimes observed along primary dendrite shafts and oblique branches (Fig. 4B), although differences in GFP-positive spine number and morphology in Les-SKF *vs*. control groups were not discernable. When sections from GFP-expressing animals were immunostained for MAP2, we observed colocalized fluorescence predominately in larger dendritic shafts and branches depending on the intensity of GFP expression, and an absence of MAP2 in spines (Fig. 4C).

Although the close clustering and low fluorescence intensity of basal processes precluded obtaining Golgi stain-like images for a full analysis of the dendritic tree, we were able to assess several aspects of apical dendrite morphology qualitatively and quantitatively using confocal images of single optical sections, and images reconstructed from stacks of optical sections spaced 1 μm apart. As shown in Fig. 4D.a, apical dendrites of Sham-SKF controls typically could be traced for nearly their entire length in single optical sections, a feature indicative of outgrowth in a straight path. In stacked projections (Fig. 4D.b), these dendrites appeared relatively straight and thick and were present in distinct bundles. In contrast, dendrites in single optical section images of Les-SKF rat mPFC appeared shortened and irregular (Fig. 4E.a), similar to their appearance when immunostained for MAP2. While bent dendrites in single sections could be seen to deviate from linearity in the x-y plane, waviness also occurred along the z-axis. Thus, only by changing the microscope focus through several different planes could these dendrites be followed from the soma to the pial surface. This is shown by stacking optical sections into projected images, revealing that dendrites that had appeared to be shortened in single sections were actually long and wavy, and followed a complete but meandering course toward layer I (Fig. 4E.b).

Photomicrographs similar to Figs. 4D & E were evaluated to compare quantitatively the degree of dendrite undulation in lesioned and sham rats treated with SKF-38393. Primary dendritic shaft lengths were measured along their visible contours within layer II/III. The linear distance between each end was also measured and a linearity index (LI) for each shaft was calculated as the ratio of the contour length to the end-to end length for each dendrite (Table 1). Whereas the average LI of primary apical dendrite shafts from Sham-SKF rats was close to 1 (or nearly linear), the LI of apical shafts from Les-SKF rats was considerably higher. Thus while the average measurements of contour and end-to-end lengths were similar between the two groups, dendritic shafts from Les-SKF rat mPFC deviated substantially from linearity and were significantly different from those of Sham-SKF. The

waviness of primary dendritic shafts was not globally present throughout the entire apical tree, as the LI of layer I branches and oblique dendrites in layers II/III and V remained unchanged. Instead, we observed a significant increase in the diameter of smaller branches in Les-SKF layers I and II/III (Table 1), a finding that appeared to correspond with the coarse and thickened MAP2 immunofluorescent staining of dendrites at the interface of layers I and II and within the neuropil of layer II/III (see Fig. 2H). In contrast, the average diameter of primary apical segments was not affected by D_1 priming.

ERK1/2 phosphorylation may play a role the development of morphological dendritic changes in mPFC of rats sensitized to a D_1 agonist

Elevated phospho-ERK immunostaining is extraordinarily prolonged in pyramidal neurons of D_1-primed rat mPFC, and coincides with a long-lasting enhancement of CREB phosphorylation in this region (Papadeas et al., 2004). Among the brain regions exhibiting sustained ERK phosphorylation, the mPFC was distinct in that phospho-ERK remained significantly elevated above baseline as long as 36 days after the final dose of D_1 agonist. In addition, a single dose of SKF-38393 at day 36 fully and stably restored phospho-ERK immunoreactivity to maximum levels in mPFC, but was less effective in other regions. Considering that ERK1/2 phosphorylation reflects a neuronal response to extracellular stimulation, these findings suggest that the mPFC is exceptionally sensitive to the neural-activating effects of D_1 priming. Since MAP kinases such as ERK participate in neural activity-dependent dendrite growth and morphology (Miller and Kaplan, 2003; Hickmott and Ethell, 2006), we investigated whether the D_1 priming-induced changes in dendrite morphology might be associated with persistent ERK phosphorylation in the mPFC of these animals.

In order to intensify phospho-ERK staining and enhance visualization of immunoreactive elements, an antigen retrieval method was employed prior to immunohistochemical staining. The overall intensity of phospho-ERK staining in neuron cell bodies, dendrites and neuropil was amplified by antigen retrieval in both Les-SKF (Fig.5A and A') and Sham-SKF (Fig. 5B and B') mPFC sections. Consistent with the results of our previous study (Papadeas et al., 2004), a pronounced increase in the number of phospho-ERK-positive cell bodies was found at day 7 in superficial and deep layers of mPFC of Les-SKF rats. Furthermore, enhancing the immunoreactivity of dendrites highlighted an increase in the number of phospho-ERK-positive apical shafts in the Les-SKF group compared to Sham-SKF rats. Many of these shafts were noticeably wavy (Fig. 5B, *arrows*), suggesting that at least some of the neurons that were morphologically abnormal were also phospho-ERK-positive. There was also a striking increase in dendritic phospho-ERK immunolabeling of layer I apical tufts in Les-SKF mPFC (Fig. 5B', *arrowheads*) compared to that of Sham-SKF animals. Preadsorption of the antibody with phosphorylated immunizing peptide (see Methods) completely blocked immunostaining in tissue sections subjected to the antigen retrieval protocol (Fig. 5C), while the non-phosphorylated peptide was without effect (Fig. 5C').

If the altered morphology of dendrites in D_1-sensitized mPFC were linked to sustained activation of ERK1/2, it might be expected that inhibition of the MEK/ERK signaling pathway would affect the development of the morphological changes. To test this hypothesis, we utilized two structurally and mechanistically dissimilar inhibitors of MEK1/2, PD98059 and SL327, administered icv 30 min prior to each weekly systemic dose of SKF-38393. As shown in Fig. 5D, icv administration of either PD98059 or SL327 prior to each dose of SKF-38393 inhibited the increase in phospho-ERK-positive cell counts (immunostained using the standard method without antigen retrieval) in mPFC of Les-SKF rats. In contrast, none of the treatments had any effect on the number of phospho-ERK-containing cells found in Sham-SKF rats.

The effect of MEK1/2 inhibitor pretreatment on MAP2 immunostaining was next examined in sections adjacent to those stained for ERK1/2. Preinfusion with either MEK1/2 inhibitor prevented the D_1 priming-induced alterations in MAP2 immunostaining in mPFC (compare preinfusion with vehicle, Fig. 5E, to preinfusion with SL327, Fig. 5E'). To quantify these findings, photomicrographs of layer II/III MAP2 immunoreactivity were used to calculate the visible area that was linear in character, represented as a fraction of the total area (linear area fraction). This method confined the area fraction measurement to only those elements that resembled apical dendrite shafts, thus quantifying the "appearance" of shortened visible dendrites in D_1-primed rats. As shown graphically in Fig. 5F, the MAP2 linear area fraction in Sham-SKF rats was not altered by preinfusion, whether the rats received 1% DMSO vehicle (Sham-Veh-SKF), or either of the MEK inhibitors dissolved in vehicle. However, in Les-SKF rats preinfused with vehicle (Les-Veh-SKF), the linear area fraction was decreased by 40 to 50%, indicating that linear MAP2-immunostained profiles in Les-Veh-SKF mPFC occupied a smaller fraction of the total stained area. On the other hand, when Les-SKF rats were preinfused with either SL327 or PD98059, the linear area fraction of apical dendrites in layer II/III was similar to that of the sham controls. These findings suggested that the apical dendrite irregularities that resulted in the shortened appearance of dendrites (due to undulations above and below the visible plane) were prevented by inhibition of the MEK1/2-ERK1/2 signaling pathway.

To assess directly the effects of MEK1/2 inhibitors on the architectural changes in D_1-primed mPFC, we administered the systemically bioavailable inhibitor SL327 (100 mg/kg ip) to GFP-transduced rats prior to each weekly injection of D_1 agonist, and examined dendrite morphology at 7 days after the last treatment. Systemic administration of the MEK inhibitor alone did not affect the architecture of dendrites in the mPFC of neonate- or sham-lesioned rats (not shown). Likewise, dendritic morphology was not altered in sham-lesioned rats injected systemically with SL327 prior to each dose of SKF-38393 (Sham-sSL-SKF, Fig. 6A). On the other hand, the loss of bundling and tortuous path of dendrites in the mPFC of Les-SKF rats was prevented by SL327 (compare Les-sVeh-SKF, Fig. 6B, to Les-sSL-SKF, Fig.6C). Quantitative analysis of photomicrographs from these animals (Fig. 6D) revealed that SL327 prevented the D_1 priming-mediated increase in the tortuosity of primary dendrites, as measured by the calculating the linearity index as described above. In addition, the increased diameter of layer I dendritic branches was inhibited in Les-sSL-SKF rat mPFC, and the diameter of layer II/III oblique dendrites was significantly reduced by the SL327 pretreatment (Fig. 6E). These findings suggest that the MEK1/2-ERK1/2 signaling pathway may be involved in promoting the altered morphology of mPFC neurons in D_1 agonist-primed rats.

DISCUSSION

Previously, we have shown that developmental lesioning of dopaminergic fibers interacts with repeated exposure to a D_1 agonist to produce neuroadaptive changes in several corticolimbic brain regions, with a remarkably protracted enhancement of ERK phosphorylation in the prefrontal cortex (Papadeas et al., 2004). Here, we have extended these findings by describing long lasting changes in the morphology of pyramidal neuron apical dendrites that is coexistent with ERK hyperphosphorylation in the mPFC of D_1-primed rats. Whereas in normal animals, long primary dendritic trunks were arranged in a characteristic parallel, bundled pattern thought to represent pyramidal neuron functional modules (Rockland and Ichinohe, 2004; but see below), this bundling pattern was disrupted in D_1-primed rat mPFC. Although apical dendritic shafts of layer V pyramidal neurons maintained a general trajectory toward the pial surface, they undulated irregularly as they coursed through layer II/III. The diameter of these primary dendritic shafts was unchanged, however their bifurcating branches at the layer I border and higher order oblique branches

within layer II/III were thickened. These structural changes were not found in the prefrontal cortices of neonate-lesioned rats treated with saline or in the mPFC of sham-lesioned rats treated with either SKF-38393 or saline. Furthermore, the effects of D_1 priming on dendritic structure in the mPFC were stable for at least three weeks after the final dose of SKF-38393, without changes in neuron cell count, laminar thickness, or in the abundance of visible primary shafts and higher order dendrites. Similar to controls, several dendritic processes of D_1-primed rats were studded with spines that appeared ostensibly normal, although further experiments will be required to adequately describe dendritic spines in these animals.

The role of pyramidal neuron apical dendritic bundling in the modular organization of the neocortex continues to be debated (Gabbot and Bacon, 1996; Rockland and Ichinohe, 2004; Krieger et al., 2007), thus it is difficult to say what implications the loss of bundling may have in the mPFC of the D_1-primed rat. Because the electrical conductance of pyramidal neurons is closely associated with dendrite diameter and branching patters (Holmes 1989; Mainen and Sejnowski, 1996; Vetter et al., 2001), it is tempting to speculate that the dendrite caliber changes we observed might cause, or might be reflective of, functional changes in the signaling properties of these neurons. The lack of early indicators of neurodegeneration such as dendritic swelling, beading or markers of proteolytic activity, combined with the maintenance of dendritic spines and increased diameter of oblique dendrites, suggest that the structural effects we observed in D_1-primed rats represent an adaptive or maladaptive response to an altered signaling environment in the mPFC, rather than a pathological indication of outright neurotoxicity. Alternatively, these observations might represent a snapshot of a neural effect that bears the potential to become either progressively degradative with continued agonist dosing, or improved over time in the absence of further stimulation. The sustained increase in immunoreactivity for phosphorylated CREB (Papadeas et al., 2004) and ERK in affected neurons suggests that the neurons retain their capacity to orchestrate signaling processes, and likely, gene transcription. Along these lines, it is interesting that that plasticity and pathology are proposed to be closely linked by a continuum of interrelated and often indistinguishable signaling events (McEachern and Shaw, 1999; Arendt, 2004; Mattson, 2007).

While the involvement of ERK1/2 in neuronal injury (Stanciu et al., 2000; Chu et al., 2004) and neuroprotection (Kaplan and Miller, 2000) is widely appreciated, recent studies propose additional roles for ERK in the regulation of dendritic structure and plasticity (Miller and Kaplan, 2003; Sweatt 2004; Chen and Ghosh, 2005). Cortical pyramidal neurons of transgenic mice expressing a constitutively active form of the upstream MEK/ERK activator p21H-ras display enhanced dendritic length, diameter and complexity (Alpar et al., 2003), as well as an increase in the phosphorylation of cytoskeletal proteins by ERK1/2 (Holzer et al., 2001). Furthermore, in primary neuronal cultures and tissue slices, ERK1/2 has been shown to mediate activity-dependent changes in dendrite structure (Quinlan and Halpain, 1996b; Wu et al., 2001; Vaillant et al., 2002). In the present study, the hypothesis that the morphological effects observed in mPFC dendrites of D_1-primed rats are related to persistent ERK hyperphosphorylation in this region is supported by several lines of evidence. First, D_1 agonist dosing was required to produce both the prolonged ERK phosphorylation and the dendritic transfiguration in neonate-lesioned rats. Second, the dendritic changes were temporally coincident with ERK phosphorylation, at least within the first 21 days after the end of the priming regimen. Third, many phospho-ERK-positive primary dendritic shafts that were traceable over some distance were conspicuously wavy. Most importantly, the administration of a MEK inhibitor prior to each dose of D_1 agonist precluded the changes in dendrite structure that occurred due to D_1 priming.

Both PD98059 and SL327 are selective inhibitors of the obligate upstream activator of ERK1/2, MEK1/2 (Alessi et al., 1995; Favata et al., 1998; Blum et al., 1999; Valjent et al.,

2000; Pearson et al., 2001). It has been proposed that U0126 (the parent compound of SL327) and PD98059 inhibit MEK by different mechanisms (Favata et al., 1998; but see Davies et al., 2000). These agents have distinct chemical structures and favorable, though slightly different selectivity profiles *in vitro* (Davies et al., 2000). Thus it is likely that the effects of these compounds in the present study were mediated by MEK1/2 inhibition and not by some common, nonspecific mechanism. Moreover, we found that these agents were similarly effective whether administered icv (in the case of PD98059 or SL327), or systemically (SL327). Taken together our findings suggest that ERK-related signaling may play a role in establishing and/or maintaining the persistent changes observed in mPFC dendrite morphology. Relating to this, preliminary studies indicate that a single dose of a MEK inhibitor, administered only following the final dose of SKF-38393, ameliorates the decreases in quantitative measures of MAP2 immunostaining observed with D_1 priming (not shown). Continuous activity by MEK1/2 may thus be required in order to maintain these structural adaptations over time.

A considerable portion of cellular ERK associates with the cytoskeleton (Fiore et al., 1993; Reszka et al., 1995). ERK1/2 may associate with microtubules and other cytoskeletal elements without directly phosphorylating them, an interaction that could serve to scaffold the ERK signaling pathway to facilitate its activity, or retain active ERK within the cytoplasm (Morishima-Kawashima and Kosik, 1996; Reszka et al., 1995). Within the dendritic cytoskeleton, phosphorylation by ERK1/2 regulates the function of many of its substrates, including MAP1, -2, and -4, neurofilament proteins and stathmin. The phosphorylation of MAP2 by ERK1/2 results in destabilization of dendritic microtubules (Sanchez et al., 2000). Such destabilization might provide one explanation for the appearance of apical dendrites in D_1-primed rats. Several kinases, including glycogen synthase kinase (GSK), calcium/calmodulin-dependent kinases (CAMKs), the MAP kinases JNK and p38, PI3-kinase and many others, cooperate in an upstream or parallel fashion with ERK1/2 to regulate cytoskeletal elements and thus affect dendrite morphology (Redmond et al., 2002; Vaillant et al., 2002 Chang et al., 2003; Miller and Kaplan, 2003; Dijkhuizen and Ghosh, 2004; Hickmott and Ethell, 2006). Further studies will be necessary to delineate the exact mechanism by which sustained ERK activation supports the adaptations observed in the mPFC of D_1-primed rats.

Immunolabeling with anti-MAP2 is frequently used as a marker for somatodendritic structures, based on its preferential expression in dendrites and neuron cell bodies, and on evidence that dendritic growth correlates with an increase in MAP2 immunostaining (Philpot et al., 1997; Sanchez et al., 2000; Bury and Jones, 2002). However, our findings suggest that some caution is necessary when interpreting MAP2 immunostaining in fixed tissue sections. Anti-MAP2 labeled large caliber primary shafts more effectively than smaller dendrites, and the waviness of these large shafts was reflected immunohistochemically as shortened and bent profiles in D_1-primed rats. By confocal reconstruction of GFP-expressing dendrites, we demonstrated that these dendrites were not shortened, but rather disappeared from the plane of view due to optical and physical sectioning of the tissue. Similarly, the diminished appearance of MAP2 immunostaining in the mPFC was not corroborated quantitatively by western blotting, but instead might be attributed partially to the loss of bundling and increased spacing between primary dendritic shafts. In the neuropil, MAP2-labeled oblique dendrites that were detected colorimetrically with DAB were less visible than when the same antibody was detected by fluorescence methods. Differences in secondary antibody affinity or greater optical sensitivity of the instrumentation for fluorescence detection might account for this discrepancy. Nevertheless, these results emphasize that careful scrutiny of MAP2 immunoreactive profiles and complementary methodology are critical to avoid misinterpretation of MAP2 findings in tissue sections.

The wavy, disorganized appearance of mPFC apical processes in D_1-primed rats bears a strong morphological resemblance to the loss of bundling and irregularly shaped dendrites observed in the frontal cortices of prenatal cocaine-exposed animals (Jones et al., 1996; Murphy et al., 1997; Stanwood et al., 2001) and D_1 receptor knockout mice (Stanwood et al., 2005). While these structural similarities and the involvement of dopaminergic signaling might invite mechanistic comparisons however, the effects are distinguishable temporally from those of adult D_1 primed rats. Disruption of dendritic profiles has been shown to be present from embryonic development in prenatal cocaine-treated animals (Jones et al., 2000), and from the early postnatal period in D_1 receptor-null mice (Stanwood et al., 2005), and is maintained into adulthood. This implies that during morphogenesis, turning growth cones responded to prevailing neurotransmitter activity by altering dendrite trajectories (Levitt et al., 1997). In contrast, mPFC pyramidal dendrites in 6-OHDA neonate-lesioned rats are normal in appearance until the animals are exposed to a D_1 agonist in adulthood; afterwards, the effects of agonist administration are maintained for several weeks following the cessation of drug treatment. These findings suggest that, like the behavioral expression of D_1 priming, a latent susceptibility for morphological disruption is established by dopamine loss during development. While homeostatic mechanisms may conceal certain behavioral and structural phenotypes in rats that undergo development without dopamine from the early postnatal period, the vulnerability for such changes to occur persists into adulthood. Subsequent exposure to a dopaminergic agonist interacts with or unmasks the potential for these outcomes, which are then manifested in an enduring manner. Within the neural circuitry that subserves dopaminergic sensitization, D_1 agonist treatment stimulates long-lasting alterations in neurochemical signaling, likely contributing to the stability of these effects.

Recent evidence implicates an interacting relationship between dopamine dysregulation, behavioral and biochemical sensitization, and environmental factors such as stress or drug exposure in the pathophysiology of several disorders involving frontostriatal circuit dysfunction (see, for example, Howes et al., 2004, and Visser et al., 2000). In Lesch-Nyhan syndrome (LNS) for example, reduced dopaminergic neuron density in the caudate-putamen and alterations in receptor sensitivity are evident early in life. Interestingly however, aggressive behavior in 10 to 20 year old Lesch-Nyhan patients has been correlated with somewhat higher residual presynaptic dopamine activity (Ernst et al., 1996). Although speculative, some of the behavioral manifestations of LNS might thus represent a sensitized response to remaining dopamine, the release of which would be subject to stimulation by stress and other external conditions. Similar behaviorally as well as neurochemically to LNS, the D_1-primed rat exhibits latent, environmentally activated (by D_1 agonist administration) hyperresponsiveness as a result of developmental dopamine loss, thus modeling critical features of LNS and other frontostriatal circuit disorders (Breese et al., 2004). Furthermore, consistent with our own studies, changes in prefrontal dendrite morphology have been identified in other animal models of these disorders (Wedzony et al., 2005; Flores et al., 2005; Mikolaenko et al., 2005; Robinson and Kolb, 2004). It is reasonable to suggest that prefrontal cortical dendritic remodeling in such disorders might reflect both consequence and cause: as an adaptation to developmental or chronic alterations in functional circuitry, and as a contributor to the behavioral impairments associated with them, respectively. The relationship between the behavioral effects of D_1 priming and dendritic changes in the mPFC will be the subject of future investigations.

Acknowledgments

We thank Dr. Robert Bagnell of UNC-Chapel Hill for advice on morphometry, Wendy Salmon of the Michael Hooker Microscopy Facility for providing technical expertise with the confocal microscopy, and the UNC Virus Vector Core for production of the recombinant AAV viruses.

Grant Support: National Institutes of Health Grants MH01896 (B.L.B.) and NS035633 (T.J.M.), and by the Lesch-Nyhan Foundation (G.R.B.)

LITERATURE CITED

Alessi DR, Cuenda A, Cohen P, Dudley DT, Saltiel AR. PD 098059 is a specific inhibitor of the activation of mitogen-activated protein kinase kinase *in vitro* and *in vivo*. J Biol Chem. 1995; 270:27489–27494. [PubMed: 7499206]

Alpar A, Palm K, Schierwagen A, Arendt T, Gartner U. Expression of constitutively active p21H-rasval12 in postmitotic pyramidal neurons results in increased dendritic size and complexity. J Comp Neurol. 2003; 467:119–133. [PubMed: 14574684]

Arendt T. Neurodegeneration and plasticity. Int J Dev Neurosci. 2004; 22:507–514. [PubMed: 15465280]

Atkins CM, Selcher JC, Petraitis JJ, Trzaskos JM, Sweatt JD. The MAPK cascade is required for mammalian associative learning. Nat Neurosci. 1998; 1:602–609. [PubMed: 10196568]

Binder LI, Frankfurter A, Rebhun LI. Differential localization of MAP-2 and tau in mammalian neurons in situ. Ann NY Acad Sci. 1986; 466:145–166. [PubMed: 3089105]

Blanchart A, De Carlos JA, López-Mascaraque L. Time frame of mitral cell development in the mice olfactory bulb. J Comp Neurol. 2006; 496:529–543. [PubMed: 16572431]

Blum S, Moore AN, Adams F, Dash PK. A mitogen-activated protein kinase cascade in the CA1/CA2 subfield of the dorsal hippocampus is essential for long-term spatial memory. J Neurosci. 1999; 19:3535–3544. [PubMed: 10212313]

Breese GR, Baumeister AA, McCown TJ, Emerick SG, Frye GD, Crotty K, Mueller RA. Behavioral differences between neonatal and adult 6-hydroxydopamine-treated rats to dopamine agonists: relevance to neurological symptoms in clinical syndromes with reduced brain dopamine. J Pharmacol Exp Ther. 1984; 231:343–354. [PubMed: 6149306]

Breese GR, Napier C, Mueller RA. Dopamine agonist-induced locomotor activity in rats treated with 6-hydroxydopamine at differing ages: Functional supersensitivity of D-1 dopamine receptors in neonatally lesioned rats. J Pharmacol Exp Ther. 1985; 234:447–455. [PubMed: 3926987]

Breese GR, Knapp DJ, Criswell HE, Moy SS, Papadeas ST, Blake BL. The neonate-6-hydroxydopamine-lesioned rat: a model for clinical neuroscience and neurobiological principles. Brain Res Brain Res Rev. 2005; 48:57–73. [PubMed: 15708628]

Bury SD, Jones TA. Unilateral sensorimotor cortex lesions in adult rats facilitate motor skill learning with the “unaffected” forelimb and training-induced dendritic structural plasticity in the motor cortex. J Neurosci. 2002; 22:8597–8606. [PubMed: 12351733]

Chang L, Jones Y, Ellisman MH, Goldstein LS, Karin M. JNK1 is required for maintenance of neuronal microtubules and controls phosphorylation of microtubule-associated proteins. Dev Cell. 2003; 4:521–533. [PubMed: 12689591]

Chen Y, Ghosh A. Regulation of dendritic development by neuronal activity. J Neurobiol. 2005; 64:4–10. [PubMed: 15884010]

Chu CT, Levinthal DJ, Kulich SM, Chalovich EM, DeFranco DB. Oxidative neuronal injury. The dark side of ERK1/2. Eur J Biochem. 2004; 271:2060–2066. [PubMed: 15153095]

Criswell H, Mueller RA, Breese GR. Priming of D1-dopamine receptor responses: long-lasting behavioral supersensitivity to a D1-dopamine agonist following repeated administration to neonatal 6-OHDA-lesioned rats. J Neurosci. 1989; 9:125–133. [PubMed: 2521511]

Criswell HE, Mueller RA, Breese GR. Long-term D1-dopamine receptor sensitization in neonatal 6-OHDA-lesioned rats is blocked by an NMDA antagonist. Brain Res. 1990; 512:284–290. [PubMed: 2162235]

Czogalla A, Sikorski AF. Spectrin and calpain: a ‘target’ and ‘sniper’ in the pathology of neuronal cells. Cell Mol Life Sci. 2005; 62:1913–1934. [PubMed: 15990959]

Davies SP, Reddy H, Caivano M, Cohen P. Specificity and mechanism of action of some commonly used protein kinase inhibitors. Biochem J. 2000; 351:95–105. [PubMed: 10998351]

Demyanenko GP, Tsai AY, Maness PF. Abnormalities in neuronal process extension, hippocampal development, and the ventricular system of L1 knockout mice. J Neurosci. 1999; 19:4907–4920. [PubMed: 10366625]

Dijkhuizen PA, Ghosh A. BDNF regulates primary dendrite formation in cortical neurons via the PI3-kinase and MAP kinase signaling pathways. J Neurobiol. 2004; 62:278–288. [PubMed: 15514998]

Ernst M, Zametkin AJ, Matochik JA, Pascualvaca D, Jons PH, Hardy K, Hankerson JG, Doudet DJ, Cohen RM. Presynaptic dopaminergic deficits in Lesch-Nyhan disease. New Engl J Med. 1996; 334:1568–1572. [PubMed: 8628337]

Favata MF, Horiuchi KY, Manos EJ, Daulerio AJ, Stradley DA, Feeser WS, Van Dyk DE, Pitts WJ, Earl RA, Hobbs F, Copeland RA, Magolda RL, Scherle PA, Trzaskos JM. Identification of a novel inhibitor of mitogen-activated protein kinase kinase. J Biol Chem. 1998; 273:18623–18632. [PubMed: 9660836]

Fiore RS, Bayer VE, Pelech SL, Posada J, Cooper JA, Baraban JM. p42 mitogen-activated protein kinase in brain: prominent localization in neuronal cell bodies and dendrites. Neuroscience. 1993; 55:463–472. [PubMed: 8377938]

Flores G, Alquicer G, Silva-Gomez AB, Zaldivar G, Stewart J, Quirion R, Srivastava LK. Alterations in dendritic morphology of prefrontal cortical and nucleus accumbens neurons in post-pubertal rats after neonatal excitotoxic lesions of the ventral hippocampus. Neuroscience. 2005; 133:463–470. [PubMed: 15878241]

Gabbott PL, Bacon SJ. The organisation of dendritic bundles in the prelimbic cortex (area 32) of the rat. Brain Res. 1996; 730:75–86. [PubMed: 8883891]

Gu Z, Jiang Q, Zhang G. Extracellular signal-regulated kinase 1/2 activation in hippocampus after cerebral ischemia may not interfere with postischemic cell death. Brain Res. 2001; 901:79–84. [PubMed: 11368953]

Haycock JW. Quantitation of tyrosine hydroxylase protein levels: Spot Immunolabeling with an affinity-purified antibody. Anal Biochem. 1989; 181:259–266. [PubMed: 2573292]

Hickmott PW, Ethell IM. Dendritic plasticity in the adult neocortex. Neuroscientist. 2006; 12:16–28. [PubMed: 16394190]

Holmes WR. The role of dendritic diameters in maximizing the effectiveness of synaptic inputs. Brain Res. 1989; 478:127–137. [PubMed: 2538199]

Holzer M, Rodel L, Seeger G, Gartner U, Narz F, Janke C, Heumann R, Arendt T. Activation of mitogen-activated protein kinase cascade and phosphorylation of cytoskeletal proteins after neurone-specific activation of p21ras. II. Cytoskeletal proteins and dendritic morphology. Neuroscience. 2001; 105:1041–1054. [PubMed: 11530241]

Howes OD, McDonald C, Cannon M, Arseneault L, Boydell J, Murray RM. Pathways to schizophrenia: the impact of environmental factors. Neuropsychopharmacol. 2004; 7(Suppl 1):S7–S13.

Johnson KB, Criswell HE, Jensen KF, Simson PE, Mueller RA, Breese GR. Comparison of the D1-dopamine agonists SKF-38393 and A-68930 in neonatal 6-hydroxydopamine-lesioned rats: Behavioral effects and induction of c-fos-like immunoreactivity. J Pharmacol Exp Ther. 1992; 262:855–865. [PubMed: 1354257]

Jones L, Fischer I, Levitt P. Nonuniform alteration of dendritic development in the cerebral cortex following prenatal cocaine exposure. Cereb Cortex. 1996; 6:431–445. [PubMed: 8670669]

Jones LB, Stanwood GD, Reinoso BS, Washington RA, Wang HY, Friedman E, Levitt P. In utero cocaine-induced dysfunction of dopamine D1 receptor signaling and abnormal differentiation of cerebral cortical neurons. J Neurosci. 2000; 20:4606–4614. [PubMed: 10844030]

Kalcheva N, Albala JS, Binder LI, Shafit-Zagardo B. Localization of specific epitopes on human microtubule-associated protein 2. J Neurochem. 1994; 63:2336–2341. [PubMed: 7525876]

Kaplan DR, Miller FD. Neurotrophin signal transduction in the nervous system. Curr Opin Neurobiol. 2000; 10:381–391. [PubMed: 10851172]

Klein RL, Hamby ME, Gong Y, Hirko AC, Wang S, Hughes JA, King MA, Meyer EM. Dose and promoter effects of adeno-associated viral vector for green fluorescent protein expression in the rat brain. Exp Neurol. 2002; 176:66–74. [PubMed: 12093083]

Krieger P, Kuner T, Sakmann B. Synaptic connections between layer 5b pyramidal neurons in mouse somatosensory cortex are independent of apical dendrite bundling. J Neurosci. 2007; 27:11473–11482. [PubMed: 17959790]

Lamprecht R, LeDoux J. Structural plasticity and memory. Nat Rev Neurosci. 2004; 5:45–54. [PubMed: 14708003]

Levitt P, Harvey JA, Friedman E, Smansky K, Murphy EH. New evidence for neurotransmitter influences on brain development. Trends Neurosci. 1997; 20:269–274. [PubMed: 9185309]

Liao J, Xu X, Wargovich MJ. Direct reprobing with anti-β-actin antibody as an internal control for Western blot analysis. Biotechniques. 2000; 28:216–218. [PubMed: 10683726]

Mainen ZF, Sejnowski TJ. Influence of dendritic structure on firing pattern in model neocortical neurons. Nature. 1996; 382:363–366. [PubMed: 8684467]

Mattson MP. Mitochondrial regulation of neuronal plasticity. Neurochem Res. 2007; 32:707–715. [PubMed: 17024568]

McCown TJ. Adeno-associated virus-mediated expression and constitutive secretion of galanin suppresses limbic seizure activity *in vivo*. Mol Ther. 2006; 14:63–68. [PubMed: 16730475]

McEachern JC, Shaw CA. The plasticity-pathology continuum: defining a role for the LTP phenomenon. J Neurosci Res. 1999; 58:42–61. [PubMed: 10491571]

Mikolaenko I, Rao LM, Roberts RC, Kolb B, Jinnah HA. A Golgi study of neuronal architecture in a genetic mouse model for Lesch-Nyhan disease. Neurobiol Dis. 2005; 20:479–490. [PubMed: 15908225]

Miller FD, Kaplan DR. Signaling mechanisms underlying dendrite formation. Curr Opin Neurobiol. 2003; 13:391–398. [PubMed: 12850225]

Minger SL, Geddes JW, Holtz ML, Craddock SD, Whiteheart SW, Siman RG, Pettigrew LC. Glutamate receptor antagonists inhibit calpain-mediated cytoskeletal proteolysis in focal cerebral ischemia. Brain Res. 1998; 810:181–199. [PubMed: 9813316]

Morishima-Kawashima M, Kosik KS. The pool of map kinase associated with microtubules is small but constitutively active. Mol Biol Cell. 1996; 7:893–905. [PubMed: 8816996]

Moy SS, Breese GR, Eckerman DA. Altered activity patterns following neonatal 6-hydroxydopamine lesions to dopaminergic neurons: Effect of SKF-38393. Brain Res. 1994; 645:49–60. [PubMed: 8062100]

Murphy EH, Fischer I, Friedman E, Grayson D, Jones L, Levitt P, O'Brien-Jenkins A, Wang HY, Wang XH. Cocaine administration in pregnant rabbits alters cortical structure and function in their progeny in the absence of maternal seizures. Exp Brain Res. 1997; 114:433–441. [PubMed: 9187279]

Papadeas ST, Blake BL, Knapp DJ, Breese GR. Sustained extracellular signal-regulated kinase 1/2 phosphorylation in neonate 6-hydroxydopamine-lesioned rats after repeated D1-dopamine receptor agonist administration: implications for NMDA receptor involvement. J Neurosci. 2004; 24:5863–5876. [PubMed: 15229233]

Pearson G, Robinson F, Beers Gibson T, Xu BE, Karandikar M, Berman K, Cobb MH. Mitogen-activated protein (MAP) kinase pathways: regulation and physiological functions. Endocr Rev. 2001; 22:153–183. [PubMed: 11294822]

Paxinos, G.; Watson, C. The Rat Brain in Stereotaxic Coordinates. 4 Edition. Academic Press; New York: 1998.

Philpot BD, Lim JH, Halpain S, Brunjes PC. Experience-dependent modifications in MAP2 phosphorylation in rat olfactory bulb. J Neurosci. 1997; 17:9596–9604. [PubMed: 9391014]

Quinlan EM, Halpain S. Postsynaptic mechanisms for bidirectional control of MAP2 phosphorylation by glutamate receptors. Neuron. 1996a; 16:357–368. [PubMed: 8789950]

Quinlan EM, Halpain S. Emergence of activity-dependent, bidirectional control of microtubule-associated protein MAP2 phosphorylation during postnatal development. J Neurosci. 1996b; 16:7627–7637. [PubMed: 8922419]

Rau SW, Dubal DB, Böttner M, Gerhold LM, Wise PM. Estradiol attenuates programmed cell death after stroke-like injury. J. Neurosci. 2003; 23:11420–11426. [PubMed: 14673006]

Redmond L, Kashani AH, Ghosh A. Calcium regulation of dendritic growth via CaM kinase IV and CREB-mediated transcription. Neuron. 2002; 34:999–1010. [PubMed: 12086646]

Reszka AA, Seger R, Diltz CD, Krebs EG, Fischer EH. Association of mitogen-activated protein kinase with the microtubule cytoskeleton. Proc Natl Acad Sci. 1995; 92:8881–8885. [PubMed: 7568036]

Robinson TE, Kolb B. Structural plasticity associated with exposure to drugs of abuse. Neuropharmacology. 2004; 47(Suppl 1):33–46. [PubMed: 15464124]

Rockland KS, Ichinohe N. Some thoughts on cortical minicolumns. Exp Brain Res. 2004; 158:265–277. [PubMed: 15365664]

Sanchez C, Diaz-Nido J, Avila J. Phosphorylation of microtubule-associated protein 2 (MAP2) and its relevance for the regulation of the neuronal cytoskeleton function. Prog Neurobiol. 2000; 61:133–168. [PubMed: 10704996]

Stanciu M, Wang Y, Kentor R, Burke N, Watkins S, Kress G, Reynolds I, Klann E, Angiolieri MR, Johnson JW, DeFranco DB. Persistent activation of ERK contributes to glutamate-induced oxidative toxicity in a neuronal cell line and primary cortical neuron cultures. J Biol Chem. 2000; 275:12200–12206. [PubMed: 10766856]

Stanwood GD, Washington RA, Shumsky JS, Levitt P. Prenatal cocaine exposure produces consistent developmental alterations in dopamine-rich regions of the cerebral cortex. Neuroscience. 2001; 106:5–14. [PubMed: 11564412]

Stanwood GD, Parlaman JP, Levitt P. Anatomical abnormalities in dopaminoceptive regions of the cerebral cortex of dopamine D1 receptor mutant mice. J Comp Neurol. 2005; 487:270–282. [PubMed: 15892099]

Sweatt JD. Mitogen-activated protein kinases in synaptic plasticity and memory. Curr Opin Neurobiol. 2004; 14:311–317. [PubMed: 15194111]

Vaillant AR, Zanassi P, Walsh GS, Aumont A, Alonso A, Miller FD. Signaling mechanisms underlying reversible, activity-dependent dendrite formation. Neuron. 2002; 34:985–998. [PubMed: 12086645]

Valjent E, Corvol JC, Pages C, Besson MJ, Maldonado R, Caboche J. Involvement of the extracellular signal-regulated kinase cascade for cocaine-rewarding properties. J Neurosci. 2000; 20:8701–8709. [PubMed: 11102476]

Van Eden CG, Uylings HBM. Cytoarchitectonic development of the prefrontal cortex of the rat. J Comp Neurol. 1985; 241:253–267. [PubMed: 2418068]

Vetter P, Roth A, Hausser M. Propagation of action potentials in dendrites depends on dendritic morphology. J Neurophysiol. 2001; 85:926–937. [PubMed: 11160523]

Visser JE, Bar PR, Jinnah HA. Lesch-Nyhan disease and the basal ganglia. Brain Res Rev. 2000; 32:449–475. [PubMed: 10760551]

Wang KK. Calpain and caspase: can you tell the difference? Trends Neurosci. 2000; 23:20–26. [PubMed: 10631785]

Wang X, Zhu C, Qiu L, Hagberg H, Sandberg M, Blomgren K. Activation of ERK1/2 after neonatal rat cerebral hypoxia-ischema. J Neurochem. 2003; 86:351–362. [PubMed: 12871576]

Wedzony K, Fijal K, Mackowiak M. Alterations in the dendritic morphology of prefrontal pyramidal neurons in adult rats after blockade of NMDA receptors in the postnatal period. Brain Res. 2005; 1062:166–170. [PubMed: 16257395]

Wu GY, Deisseroth K, Tsien RW. Spaced stimuli stabilize MAPK pathway activation and its effects on dendritic morphology. Nat Neurosci. 2001; 4:151–158. [PubMed: 11175875]

Zilles, K.; Wree, A. Cortex: areal and laminar structure. In: Paxinos, G., editor. The Rat Nervous System. 2nd ed.. Academic Press; San Diego, CA: 1995. p. 649-688.

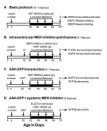

Fig. 1.

Experimental timelines for animal treatments and analyses. For each study, the number of experimental subjects is provided in parentheses, and tissue analyses performed post-sacrifice are indicated on the right. All experiments consisted of 6-OHDA or sham lesioning on PND 4, followed by behavioral priming with weekly treatments of SKF-38393 or saline beginning at PND 42 (*arrows over darkened band*). Locomotor activity was monitored immediately following each dose. Seven days after the final treatment, animals were perfused transcardially (*S*), except for a subset of subjects in study **A** that were sacrificed on PND 84 (21 days after the final dosing, as indicated with an *asterisk*). In **B**, cannula implantation (*CI*) was performed on PND 35 to prepare for preinfusions with MEK inhibitor. Preinfusions were administered 30 min prior to each weekly dose of SKF-38393. To transduce neuronal GFP expression, rats in 2 studies (**C** and **D**) received prefrontal cortical injections of AAV-GFP at PND 30 (*GFP*), followed by agonist dosing beginning on PND 42. In study **D**, animals expressing GFP were pretreated with systemic injections of SL-327, 30 min before each dose of SKF-38393.

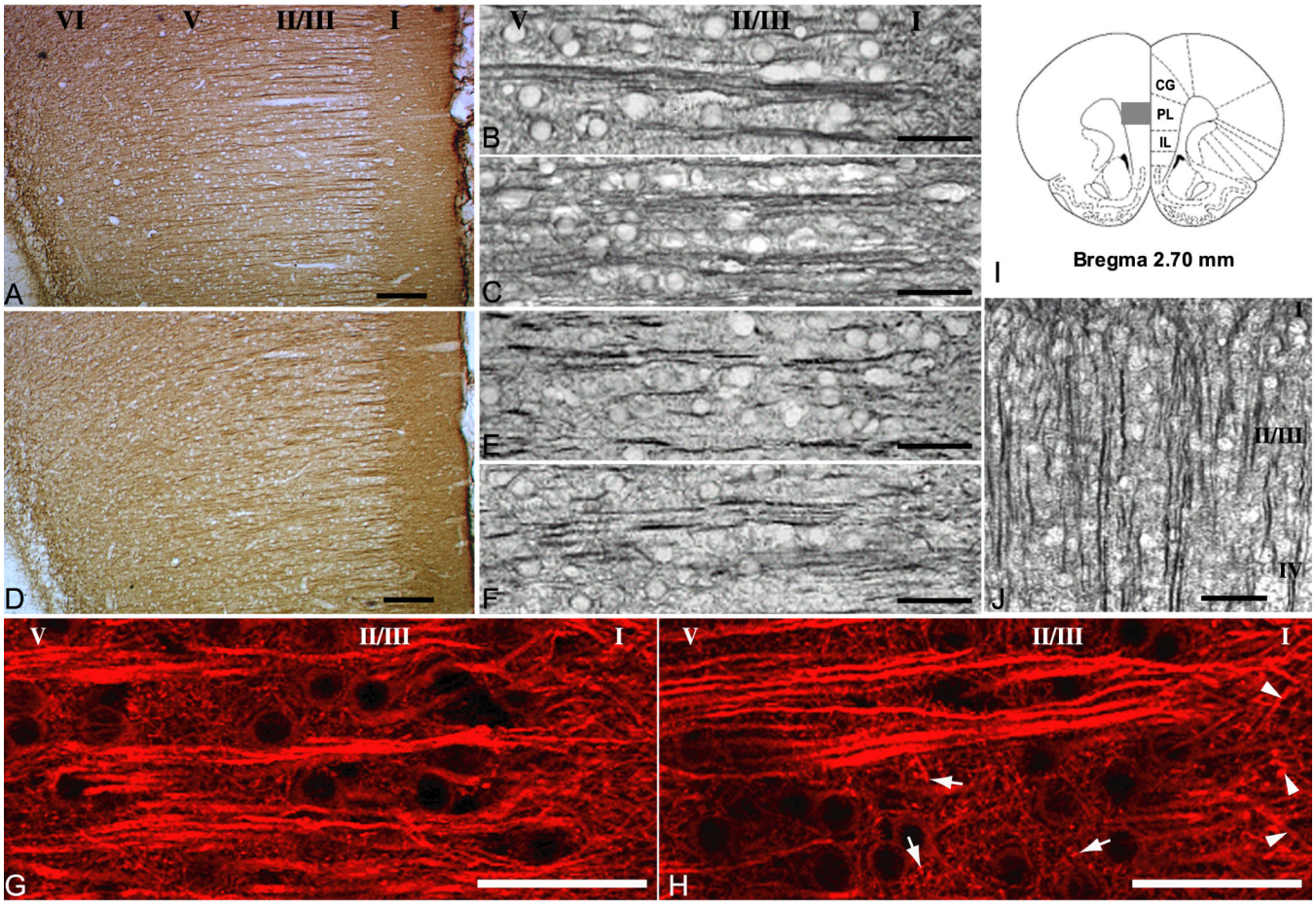

Fig. 2.

MAP2 immunohistochemistry is altered in mPFC of D_1-primed rats. Roman numerals indicate approximate location of cortical layers. All animals were euthanized 7 d after the last dose of SKF-38393 or saline except where indicated. **(A)** Representative mPFC section from a sham-lesioned rat treated with weekly injections of saline (Sham-Sal). **(B)** Higher power image from the same region in a sham-lesioned rat treated with weekly injections of SKF-38393 (Sham-SKF). **(C)** Neonate-lesioned rat treated with weekly injections of saline (Les-Sal). **(D, E)** Lesioned rat treated with weekly injections of SKF-38393 (D_1-primed, Les-SKF). **(F)** MAP2 in a Les-SKF rat euthanized 21 d after the final dose of SKF-38393. **(G, H)** Confocal images of MAP2 immunofluorescence in Sham-SKF and Les-SKF rat mPFC, respectively. Note the coarser, more granular appearance of punctate elements in the neuropil of primed rats (*arrows* in **H**), and the thickening of dendritic branches at the interface of layers II/III and I (*arrowheads* in **H**) compared to those of control rats. **(I)** Schematic diagram of region of interest, adapted from Paxinos and Watson (1998). *Gray box* represents area depicted in **A** and **D**. **(J)** MAP2 immunostaining in Les-SKF visual cortex was unaltered. Scale bars for **A**, **D** and **J**, 100 μm. Scale bars for **B**, **C** and **E**-**H**, 50 μm. Note: a magenta-green version of this figure can be viewed online as Supplementary Figure 1.

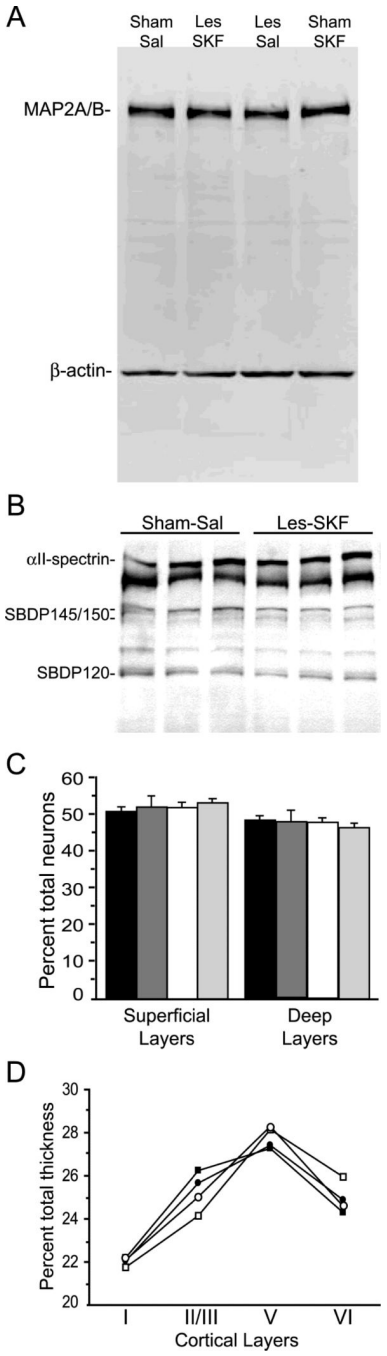

Fig. 3.

MAP2, αII-spectrin, total cell counts and cortical thickness are all unchanged in mPFC of D_1-primed rats. **(A)** Representative Western blot of MAP2 and β-actin in mPFC of SKF-38393-treated sham (Sham-SKF) and lesioned rats (Les-SKF) and their saline-treated counterparts (Sham-Sal and Les-Sal, respectively). Faint bands in the center of each lane are consistent with MAP2 degradation products. **(B)** Spectrin and its breakdown products (SBDPs) in mPFC homogenates from Sham-Sal and Les-SKF rats. Neither the 145-150 kDa calpain-mediated cleavage products, nor the 120 kDa caspase-3 SBDP were altered by D_1 priming. **(C)** Cresyl violet-stained neurons counted at day 21 after dosing across superficial (I-III) and deep (V-VI) mPFC layers. Data are expressed as percent of total cell counts

across all layers: *black bars*, Sham-Sal, 4810.5 ± 130.7 total cells; *dark gray bars*, Sham-SKF, 4237.7 ± 289.2 cells; *white bars*, Les-Sal, 4781.0 ± 441.9 cells; *light gray bars*, Les-SKF, 4326.5 ± 269.2 cells counted across all layers. **(D)** Mean cortical layer thickness at day 21 plotted as percent of total mPFC thickness. *Filled squares*, Sham-Sal; *filled circles*, Sham-SKF; *open squares*, Les-Sal; *open circles*, Les-SKF.

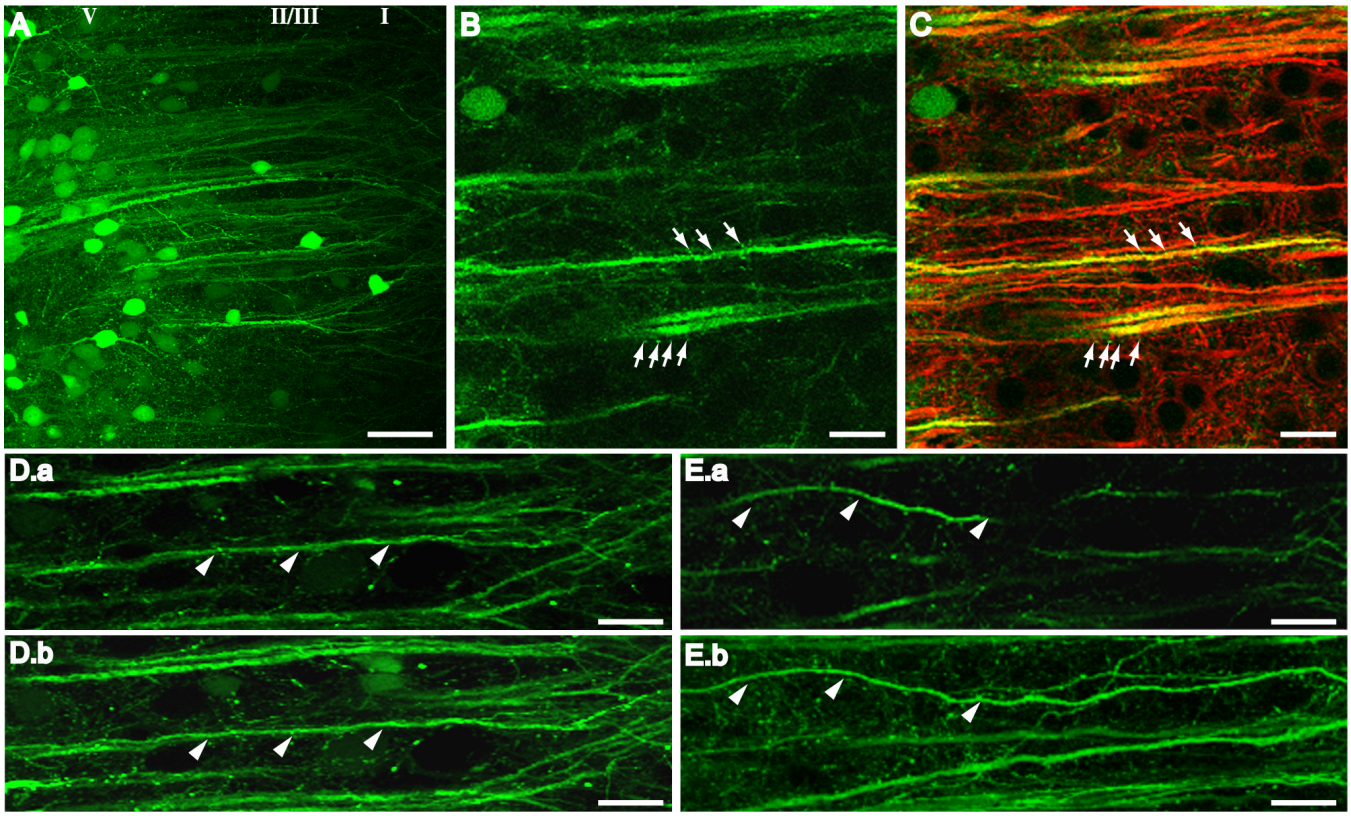

Fig. 4.

Confocal imaging of mPFC neurons transduced with AAV-GFP. **(A)** Clusters of fluorescent neurons surrounding the injection site in Sham-SKF mPFC. Prominent first order dendrites were long and straight, branching into tufts at the interface of layers II/III and I. **(B)** Representative high power image of GFP-positive dendrites in mPFC of a Les-SKF rat sacrificed at day 7 after the priming regimen. *Arrow*s indicate the presence of dendritic spines. **(C)** Overlay of the image in **B** with the corresponding image of MAP2 immunofluorescence showing colocalization in larger dendritic shafts but not in spines (*arrows*). **(D)** Image of a single 1 μm optical section **(D.a)**, and the corresponding reconstructed projection of 10 optical sections **(D.b)**, of Sham-SKF mPFC. Most dendrites are visible along their entire length in both single slice images and projections (indicated by *arrowheads*). **(E)** Single 1 μm optical section **(E.a)**, and corresponding stacked reconstruction **(E.b)**, of dendrites in Les-SKF mPFC. Several dendrites disappeared out of the single section images (*arrowheads* in **E.a**), and could only be followed for their entire length by stacking multiple images as shown in **E.b**. Scale bar for A, 50 μm. Scale bar for B-E, 20 μm. Note: a magenta-green version of this figure can be viewed online as Supplementary Figure 2.

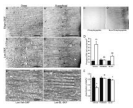

Fig. 5.

Sustained ERK phosphorylation may contribute to mPFC morphological abnormalities in D_1-primed rats. Antigen retrieval was used to intensify phospho-ERK staining in Sham-SKF **(A** and **A')** and Les-SKF (**B** and **B'**) mPFC. Note the wavy phospho-ERK-positive dendritic shafts (*arrows*) and enhanced immunostaining of dendrite apical tufts (*arrowheads*) in sections from Les-SKF (D_1-primed) rat mPFC compared to that of Sham-SKF. Scale bars, 200 μm. Specificity of the antibody under antigen retrieval conditions is shown by abolition of staining using a phosphorylated (**C**), but not a non-phosphorylated (**C**') blocking peptide. **(D)** MEK inhibitors administered prior to each weekly dose of SKF-38393 prevented the sustained increase in phospho-ERK observed at day 7 in D_1-primed rats. Sham-lesioned (*filled bars*) and neonate-lesioned (*open bars*) animals were administered icv infusions of vehicle, PD98059 or SL327, 30 min before each weekly systemic injection of SKF-38393. Cell counts were obtained from mPFC sections immunostained for phospho-ERK without antigen retrieval and represent total counts across all cortical layers. Represented are means ± S.E.M. ** $p < 0.0001$ *vs*. sham-lesioned rats preinfused with vehicle prior to SKF-38393 (Sham-Veh-SKF); ‡‡‡ $p < 0.0001$ *vs*. D_1-primed rats preinfused with vehicle (Les-Veh-SKF). **(E** and **E')** Representative photomicrographs of MAP2 immunohistochemistry in Les-Veh-SKF and Les-SL-SKF mPFC, respectively. Scale bars, 50 μm. **(F)** Quantitative analysis of MAP2 immunostaining using linear area fraction measurements. The format of the graph is the same as in **D**. Preinfusions of either PD98059 or SL327 had no effect in sham rats treated with SKF-38393 (*filled bars*), but prevented the loss of linear dendritic immunostaining in lesioned rats that were primed with the agonist (*open bars*). * $p < 0.001$ *vs*. Sham-Veh-SKF; ‡‡ $p < 0.001$, and ‡ $p < 0.05$ *vs*. Les-Veh-SKF; ANOVA with Fisher's PLSD.

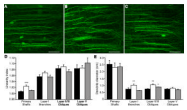

Fig. 6.

Systemic treatment with SL327 prevents the structural abnormalities induced by D_1-priming. Rats were administered 100 mg/kg ip SL327 (sSL) or vehicle (sVeh), 30 min prior to each weekly dose of SKF-38393 and sacrificed 7 days following the final treatment. **(A-C)**, Reconstructed confocal images of GFP-positive dendrites in Sham-sVeh-SKF **(A)**, Les-sVeh-SKF **(B)**, and Les-sSL-SKF **(C)** rat mPFC. Scale bars, 50 μm. **(D)** Linearity index of dendritic elements in GFP-expressing mPFC of Sham-sVeh-SKF (*black bars*), Les-sVeh-SKF (*open bars*), and Les-sSL-SKF rats (*gray bars*). Represented are means ± S.E.M. *** $p < 0.0001$ *vs*. Sham-sVeh-SKF. **(E)** Diameter of dendritic elements in mPFC. The format is the same as in **D**. ** $p < 0.005$, and * $p < 0.05$ *vs*. Sham-sVeh-SKF; ANOVA with Fisher's PLSD.

Table 1

Effects of D_1 priming on linearity index and diameter of GFP-expressing dendrites in mPFC

	Average Contour Measurement	Average End-to-end Measurement	Linearity Index	Diameter
Primary shafts				
Sham-SKF	154.98 ± 3.93	154.37 ± 4.03	1.004 ± 0.001	2.44 ± 0.31
Les-SKF	151.47 ± 6.10	148.55 ± 6.26	1.019 ± 0.002**	2.29 ± 0.40
Layer I branches				
Sham-SKF	47.93 ± 2.59	45.67 ± 2.49	1.052 ± 0.004	0.77 ± 0.06
Les-SKF	46.69 ± 1.63	44.01 ± 1.57	1.065 ± 0.008	1.11 ± 0.09*
Layer II-III obliques				
Sham-SKF	30.16 ± 0.94	28.07 ± 0.83	1.076 ± 0.007	0.76 ± 0.02
Les-SKF	30.31 ± 1.43	28.09 ± 1.42	1.085 ± 0.009	1.06 ± 0.12*
Layer V obliques				
Sham-SKF	24.23 ± 2.12	22.55 ± 1.88	1.075 ± 0.014	0.73 ± 0.02
Les-SKF	27.71 ± 0.98	25.76 ± 0.83	1.077 ± 0.006	0.79 ± 0.05

To obtain the linearity index, the contour length of each dendrite was divided by the length of a straight line from one end of the dendrite to the other. Diameter was measured at 2-3 different sites along the visible length and averaged for each dendrite. See Methods for total numbers of dendrites measured per animal. Each measurement was averaged per animal and data are expressed as the mean ± SEM of all animals per group. Sham-SKF, n = 3-4. Les-SKF, n = 5-6. Rats were perfused at day 7 after the final treatment with SKF-38393.

** $p < 0.0001$

* $p < 0.005$ *vs.* Sham-SKF.